LUND UNIVERSITY

Localization of Sunitinib in in vivo Animal and in vitro Experimental Models by MALDI Mass Spectrometry Imaging

James, Connell; Sugihara, Yutaka; Török, Szilvia; Döme, Balázs; Fehniger, Thomas; Marko-Varga, György; Végvári, Ákos

Link to publication

Total number of authors:
7

Localization of Sunitinib in *in vivo* Animal and *in vitro* Experimental Models by MALDI Mass Spectrometry Imaging

James Connell[1][†], Yutaka Sugihara[2], Szilvia Török[3,4], Balázs Döme[3,4,5,6], József Tóvári[7], Thomas E. Fehniger[1,8], György Marko-Varga[1,8,9], Ákos Végvári[1,10*]

[1]Clinical Protein Science & Imaging, Department of Biomedical Engineering, Lund University, Lund, Sweden.
[2]Department of Oncology, Clinical Sciences, Lund University and Skåne University Hospital, 221 85 Lund, Sweden
[3]National Korányi Institute of Pulmonology, Budapest, Hungary
[4]Department of Thoracic Surgery, Medical University of Vienna, Austria
[5]Department of Thoracic Surgery, Semmelweis University-National Institute of Oncology, Budapest, Hungary
[6]Department of Biomedical Imaging and Image-guided Therapy, Medical University of Vienna, Austria
[7]Department of Experimental Pharmacology, National Institute of Oncology, Budapest, Hungary
[8]Center of Excellence in Biological and Medical Mass Spectrometry, Lund University, Lund, Sweden
[9]First Department of Surgery, Tokyo Medical University, 6-7-1 Nishishinjuku Shinjuku-ku, Tokyo, Japan
[10]CREATE Health, Lund University, Lund, Sweden

[†]Permanent address: Biomedical Science, Dublin Institute of Technology, Kevin Street, Dublin, Ireland.

Address all correspondence to:
Ákos Végvári, PhD; Clinical Protein Science & Imaging, Dept. of Biomedical Engineering, Lund University, Biomedical Center D13, SE-221 84 Lund, Sweden; Phone: +46-46-222-3721; Email: akos.vegvari@bme.lth.se

Abstract

The spatial distribution of an anti-cancer drug and its intended target within a tumor plays a major role on determining how effective the drug can be at tackling the tumor. This study provides data regarding the lateral distribution of sunitinib, an oral antiangiogenic receptor tyrosine kinase inhibitor using an *in vitro* animal model as well as an *in vitro* experimental model that involved deposition of a solution of sunitinib onto tissue sections. All tumor sections were analyzed by matrix-assisted laser desorption/ionization mass spectrometry imaging and compared with subsequent histology staining. Six tumors at four different time points after commencement of *in vivo* sunitinib treatment were examined to observe the patterns of drug uptake. The levels of sunitinib present in *in vivo* treated tumor sections increased continuously until day seven but a decrease was observed at day 10. Furthermore, the *in vitro* experimental model was adjustable to produce a drug level similar to that obtained in the *in vivo* model experiments. The distribution of sunitinib in tissue sections treated *in vitro* appeared to agree with the histological structure of tumors suggesting that this approach may be useful for testing drug update.

1. Introduction

Colorectal cancer (CRC) is one of the most common causes of cancer-related death in the western world [1,2] with a strong environmental association [3]. While the 5-year survival rate for metastatic colorectal cancer is approximately 10% [1], chemotherapy alone can produce a median survival of about 20 months [4-6]. Fluorouracil has been commonly used to treat CRC for a long time but new drugs appeared recently, including cetuximab, bevacizumab, irinotecan, oxaliplatin, and capecitabine. The inhibition of angiogenesis is one of the most promising therapies for CRC as the inhibition of vascular endothelial factor (VEGF) can significantly improve survival in patients treated with the humanized monoclonal antibody, bevacizumab [7,8]. Further studies have revealed that the coordinated inhibition of platelet-derived growth factors (PDGF) is essential in modulating angiogenesis and inducing production of VEGF leading to reduced tumor vascularization and improved tumor regression [9,10].

Sunitinib is an oral antiangiogenic receptor tyrosine kinase inhibitor (previously known as SU11248, Pfizer®) [11,12]. It can block the intracellular signaling and kinase-dependent functions of VEGF and PDGF receptors. Inactivation of these signaling pathways is thought to reduce angiogenesis and tumor growth [11]. Sunitinib is commonly used or tested in the treatment of gastrointestinal stromal tumor [13], pancreatic neuroendocrine tumors [14], meningioma [15], renal cell carcinoma [11], metastatic breast cancer [16] and non-small cell lung cancer [17]. In preclinical CRC models, sunitinib demonstrated single-agent antitumor activity at well-tolerated doses. However, a phase II trial of sunitinib was discontinued due to its efficacy [18], underlining the importance of ability to predict efficacy during drug development.

A key event in the drug development process is the linking of specific disease mechanisms to targets, which is interconnected with the target-drug binding properties and directly related to the pharmacokinetic and the pharmacodynamic properties of any given drug compound [19]. It is important that an *in vitro* experimental model closely correlates with the corresponding *in vivo* model in order to be able to prove its applicability. The spatial localization of the drug is dictated by binding affinity to its target molecules in tissue, most commonly protein receptors

[19]. Matrix-assisted laser desorption/ionization mass spectrometry imaging (MALDI-MSI) is a technology that allows for the simultaneous mapping of peptides, proteins or molecules in thin tissue sections with a lateral resolution of up to 30-50 μm [20]. MALDI-MSI also has the added advantage of not being dependent on supplementary labels (*i.e.,* on the use of drug compounds with modified chemical structure). Despite its lower resolving power compared to autoradiography, in tissue studies MALDI-MSI has the unique advantage of delivering the absolute mass identity of intact compounds, their molecular fragments and metabolites (thus information that are not available in other imaging technology studies [21].

The first study utilizing MALDI-MS for the detection of a drug compound directly from tissue has profiled human ovarian tumor sections treated with paclitaxel, and also rat liver tissue spiked with spiperone [22]. Later on the technique was further developed to map the localization of orally administered anti-tumor drug substances in rat brain and in mouse tumor tissue using MALDI-MS for sampling the tissue sections in an array of positions with predefined step size [23]. Subsequent studies have focused on the localization of active compounds and its metabolites in animal models and in different biological tissues [24,25]. The MALDI-MSI technology has been applied for monitoring drug distribution kinetics in animal models as summarized by Prideaux and Stoeckli [26]. As the quantitative aspect of the technique has been explored, various normalization methods [27,28] and quantitation approaches were introduced [29-34].

The drug distribution in tissue is an important pharmacological property, identifying the accumulation sites and providing valuable information about whether the drug may be affective or toxic [35]. Because *in vivo* animal models for displaying drug distribution are time-consuming to develop and may require many experimental animals to be involved, we introduced an *in vitro* approach that employs drug deposition onto the tissue sections [21]. In this study, our goal was to verify the *in vitro* method in comparison with matched *in vivo* experiments using sunitinib in a colorectal mouse model. We have found that sunitinib localization correlated closely in the *in vitro* and *in vivo* models that may promote the use of the *in vitro* model for drug development and pre-clinical studies in the future.

2. Materials and Methods

  2.1. *In vivo* Mouse Model

Tumors were obtained from 10-week-old female Balb/C mice, which were inoculated subcutaneously with $2x10^6$ cells from the mouse colon-26 (C-26) adenocarcinoma cell line from Cell Line Service (CLS, Mason Research Institute), cultured in RPMI 1640 with 10% fetal bovine serum (FBS) and 1% penicillin/streptomycin (all from Sigma Aldrich, Steinheim, Germany) at 37°C, 5% CO_2 in a humidified atmosphere, as described previously [36]. The treatment began 2 weeks after tumor cell injection and was performed once daily at a dose of 100 mg/kg per mouse with a feeding tube for 10 consecutive days. Sunitinib (LC Laboratories (Woburn, MA, USA) at >99% purity (CAS. No. 557795-19-4) was suspended in 2% carboxymethylcellulose with 2 mg/mL methyl-4-hydroxibenzoate (both from Sigma Aldrich). Control mice received only the suspending medium. Animals were sacrificed at different time points but always 2 hours after the final drug treatment. Tumors were surgically removed, snap frozen by submerging the tissues into liquid nitrogen cooled isopentane, as described previously [37] and stored at -80°C until sectioning. All animal-model protocols were carried out in accordance with the Guidelines for Animal Experiments and were approved for the Department of Experimental Pharmacology in the National Institute of Oncology, Budapest, Hungary (permission number: 22.1/722/3/2010).

  2.2. Tissue Sectioning

Tumors were removed from the -80ºC freezer and placed in the -20ºC freezer for an hour before cutting at -20ºC in a cryostat (Leica CM1950 Cryostat, Nussloch, Germany). To avoid polymer interference in mass spectra originating from optimal cutting temperature media, the tumors were mounted on the block using distilled water. The tumors were then trimmed at 50 μm until a full surface was visible, after which 10-μm sections were cut onto glass slides (Thermo Superfrost, Thermo Scientific, Germany) and stored at ambient temperature and pressure until further use.

  2.3. *In vitro* Experimental Model

In the *in vitro* model (immersion overlay) sunitinib was deposited on the tissue surface as described earlier [21]. In brief, a tissue paper was placed on the bottom section of the moisture chamber and moistened using distilled water while the tumor

section on slide was placed in top section of the moisture chamber. Tissue sections then were covered with 125 µL of 1 µg/mL (2.5 µM) sunitinib solution in 50% methanol (MeOH) that was pipetted onto the tissue surface and incubated for 1 h at room temperature. Following incubation, the *in vitro* treated tissue surface was washed by pipetting 3 mL of 50% methanol and 3 mL of distilled water across the surface of the tissue. To confirm that non-specific binding was removed, a tissue section was washed by dipping slide into 50% MeOH and agitating the slide in methanol for 5 min followed by 20 s wash using deionized water. The sections were allowed to dry prior deposition of matrix.

2.4. Sample Preparation

The matrix was made from α-cyano-4-hydroxycinnamic acid (CHCA, Sigma Aldrich, Steinheim, Germany) at a concentration of 7.5 mg/mL in 50% acetonitrile at hypergrade for LC-MS (Merck, Darmstadt, Germany), 0.1% trifluoroacetic acid (TFA, Sigma-Aldrich, Steinheim, Germany) and was made up fresh every week. The airbrush which was used to spray the matrix was kept in a fume hood for safety. The airbrush was run off compressed nitrogen. One mL of CHCA matrix solution was added to an Aztek A470 airbrush (Testor Corp. Rockfort, IL) and sprayed in short burst fashion on to each tissue section. The tissue sections were held 10-12 cm from the airbrush nozzle and a 3-5 s gap in between each spray was allowed for the matrix to dry and crystallize on the surface [38]. After the matrix was applied, the slide had a yellow frosted appearance and the tissue section was covered with matrix.

2.5. MALDI Mass Spectrometry Imaging Analysis

The MALDI-MS acquisition was performed in a MALDI LTQ Orbitrap XL mass spectrometer (Thermo Fisher Scientific, Bremen, Germany) using a method that employed 10-10 laser shots at 10 µJ for 2 scan events. Automatic gain control was switched off. The tissue surface was sampled in meandering mode at 100-µm distance between positions. First, full scans in profile mode in a mass range from *m/z* 200 to 500 were generated in the Orbitrap at resolution of 60,000 (at *m/z* 400) in positive polarity. The second scan event producing collision induced dissociation (CID) fragmentation MS/MS spectra in a mass range from *m/z* 105 to 500 was performed in the linear ion trap in positive polarity.

2.6. Data Visualization

The raw files were opened using ImageQuest™ software (Thermo Fisher Scientific, San José, CA) and the precursor or fragment ion masses of sunitinib were extracted showing their localization within the tissue sections. Screen shots were taken of the distribution of sunitinib precursor ion (*m/z* 399.218) normalized on total ion count (TIC) and of its product ion (*m/z* 326.1) at maximum image resolution allowed. For estimation of sunitinib concentrations in tissue sections, the normalized precursor ion maps of *m/z* 399.218 were used. The average signal intensity of five non-overlapping ROIs (sized 1 x 1 mm of each containing 100 positions) randomly distributed over the analyzed surface was determined in each tissue section after 1, 4, 7 and 10 days treatment using the rectangular averaging function of ImageQuest™.

2.7. Histological Staining

Slides were dipped in and out of 70% ethanol until they turned clear. After removal of the matrix, the slides were immersed in 4% phosphate buffered formaldehyde (Histolab, Gothenburg, Sweden) for 30 minutes, which was followed by a distilled water wash for 5 s. The slides were then immersed in Meyer's hematoxylin (Histolab, Gothenburg, Sweden) for 3 minutes, followed by a blueing in running water for 10 min. Staining in eosin (Histolab, Gothenburg, Sweden) for 1 min was followed by a wash with deionized water. Then the slides were dipped in 70% ethanol (Histolab AB, Gothenburg, Sweden) for 30 s, in 90% ethanol for 1 min and in 100% ethanol for 1 min. Following the slides were put in 4 different xylene (VWR, Stockholm, Sweden) baths for 1 minute in each bath and finally were cover slipped by applying Pertex® (Histolab AB, Gothenburg, Sweden) to a cover slip.

Cover slipped H&E-stained slides were loaded into the slide scanner (Mirax Midi Slide Scanner, Zeiss, Germany) to take a non-detailed image for selection of regions of interest to be scanned at high resolution. The files were opened in Aperio ImageScope Viewer v12.1 (Leica Biosystems Imaging Inc., Vista, CA), where a photo of the detailed H&E scan could be taken and saved as a *.tiff* image file.

3. Results and Discussion

3.1. Sunitinib Localization in Treated Tumors – *In vivo* Model

Animal models of cancer cell lines are valuable tools in understanding disease progression and also in drug therapy developments. We have used a mouse colorectal model that was induced by injecting C-26 adenocarcinoma cells subcutaneously. Following two weeks of tumor growth, three mice were treated with a single dose of *per os* sunitinib (100 mg/kg). The animals were sacrificed after 2 h and their tumors were removed surgically and snap frozen. These treated tumors were selected to investigate sunitinib distribution in tissue sections expecting that the single dose of drug treatment had minimal effect on tumor histology. All tumors appeared with similar histological characteristics displaying homogeneous distribution of cancer cells within the tissue sections as shown in the H&E panels of **Figure 1**. Three adjacent tissue sections from the middle region of each tumor were subjected to MALDI-MS imaging using CHCA as matrix.

The ionization of sunitinib was characterized in pure solution (dissolving 1 mg sunitinib in 50% MeOH) spotted and mixed with 3 mg/mL CHCA on MALDI target plate. Precursor and product ions of sunitinib were recognized at *m/z* 399.218 (accurate mass by Orbitrap) and *m/z* 326.1 and 283.1 (obtained by ion trap), respectively. The distribution of drug signals was found to be similar in three tissue sections of a tumor treated with a single dose of sunitinib. Typically the highest levels of sunitinib were observed in the peripheral areas of the tumor as the extracted ion chromatograms (XIC) of precursor mass (*m/z* 399.218) normalized on TIC showed in **Figure 1** (middle panels). The identification of sunitinib in tissue section was verified by a second scan event in each pixel generating tandem mass spectra. The XIC of the most intensive product ion (*m/z* 326.1), as shown in the right panels of **Figure 1**, displayed excellent co-localization with the precursor mass. The levels of drug in the C-26 adenocarcinoma clearly indicated that the drug could be absorbed in the tissue section.

We have investigated whether this specific distribution of sunitinib in treated tumor sections might be a result of technical artifacts related to matrix deposition. An untreated tumor section was prepared applying the same protocol, spraying 7.5 mg/mL CHCA onto the tissue surface (**Figure 2A**). As expected, no sunitinib signal (detected as precursor mass at *m/z* 399.218) was detected over the tissue section as shown in **Figure 2B**. Furthermore, the matrix signal, clearly observed as Na-adduct

[M+Na]$^+$ at *m/z* 212.032, was distributed rather homogeneously on the tissue surface with significantly lower intensities compared to the sampled area on the glass slide only (**Figure 2C**). However, the peripheral area of the tissue displayed no specific crystallization properties or higher matrix signals, indicating that sunitinib distribution was specific and not due to technical artifacts.

We have also investigated the crystallization optically in two regions of interest (ROIs) using transmission microscopy with a fluorescent filter at 50-fold magnification as shown in **Figure 2**. The size of matrix crystals was smaller and the layer was more homogeneous in ROI$_2$ than in ROI$_1$. The mapped signals of the matrix (Na-adduct) in the ROIs revealed that the crystallization was somewhat less heterogeneous and lower signal levels were detected in the tissue section (ROI$_1$) than that from the glass surface (ROI$_2$).

The comparison of two additional tumors identically treated with a single dose of sunitinib exposed similar peripheral distribution in one sample with lower signal intensities (**Figure 3A**) compared with the tumor presented in **Figure 1**. However, the third tumor showed sunitinib localization somewhat more homogeneously and also the average signal intensity was the highest among the three biological replicates (**Figure 3B**). The variation of the sunitinib levels may be due to differences in individual drug uptake rate after receiving a single doze.

3.2. Temporal Distribution of Sunitinib in Treated Tumors – *In vivo* Model

Obviously*, in vivo* experiments are needed if the temporal distribution of the drug is a subject of investigation. Continued treatment with sunitinib has demonstrated that the drug could accumulate in the entire tumor as high levels of the active compound was detected more homogeneously in the center of tissue sections already after 4 days of administration (data not shown). The measured levels of sunitinib were estimated by averaging the signal intensities of the normalized precursor ion (*m/z* 399.218) in five smaller sized DOIs in each tissue section and compared in tumors treated for different periods of time as shown in **Figure 4**. A continuous increase of sunitinib signal was obtained between day one and seven, while the last time point at day 10 showed a significantly lower intratumoral drug level. The increase in levels may be caused by the drug entering the mouse tumor faster than the tumor cells can metabolize and

excrete the drug, that will then reach a saturation at a time point between day 7 and day 10. Similar effect was observed previously studying saturation of drug binding sites [39].

3.3. Sunitinib Localization in Untreated Tumors – *In vitro* Model

The *in vitro* model was adjusted to detect similar levels of sunitinib to those of the *in vivo* method. Sections from untreated tumors were used to investigate drug distribution following overlay of sunitinib solution for 1 h and washing with MeOH and water. The concentration of sunitinib and optimal incubation time was determined with different concentrations of sunitinib solutions applied onto the surface of different tissue sections from an untreated tumor at concentrations of 1000, 100, 10, 1 and 0.1 µg/mL in 50% MeOH. The concentration of 1 µg/mL (2.5 µM) was found to be most suitable for detection with similar signal intensities to the *in vivo* levels. Triplicates of tissue sections from each tumor were then covered with 1 µg/mL sunitinib according to the experimental immersion overlay protocol and applied throughout the entire study in *in vitro* model.

In comparison of the *in vivo* and *in vitro* models, similar levels of sunitinib with a homogenous distribution were observed in two tumors treated *in vitro* (**Figure 5**). Although both tumors were treated identically with the same volume and concentration of drug and were analyzed using the same method, the drug signals were higher in the lower area of the second tumor (**Figure 5B**). Nevertheless, the immersion overlay apparently provided satisfactory results in terms of detectable signal intensities, as well as the drug adequately covered and distributed in the tissue sections after washing. The fact that the drug was deposited onto thin tissue sections of the tumor allowed the compound to directly access the cytoplasm without passing through the cell membrane. Additionally, the high concentration of organic modifier (50% MeOH) in the sunitinib solution might alter the conformation of many proteins and thus enabling new interaction sites and increasing non-specificity.

Comparing the *in vivo* and the immersion overlay *in vitro* model, a similarity between the distributions of sunitinib was found. The immersion overlay model has the strongest resemblance to the treated tissue sections at later stage when sunitinib is

fully diffused into the tumor. However, subtle biological differences in the tumors may contribute to the specific localization and the detected signal intensities of the drug. Individual variations may also be explained by a quenching factor present in a tumor that is not present in the other, which is amplifying or muting the signal from MALDI-MSI. It is generally accepted that ion suppression can be caused by a variety of factors, including salts, ion pairing agents, exogenous compounds, metabolites or proteins [40] as well as by the tissue type [41]. Increased intratumoral ion suppression may be caused by one or a combination of these factors, such as dehydration leading to increased salt levels in the tissue. Levels of drug in the tumor may be also affected by some of the drugs side effects such as diarrhea [42]. Furthermore, it is possible that the mice may have not been able to absorb the entire given dose resulting in reduced levels of detected drug in the tumors.

By this series of experiment we intended to investigate if our *in vitro* model could recapitulate the *in vivo* model when the major question was whether the active compound could enter the tumor and reach its target receptors in tumor cells. Based on the similarities in sunitinib distribution in the *in vivo* treated tumor samples and in the *in vitro* model, we conclude that the latter experimental setting has the potential to be used to investigate or predict whether a drug can interfere with a tissue surface expressing specific target proteins. A combination of drug solution may also be investigated hence to provide fast predictive information how compounds could be combined to improve treatment efficiency.

4. Conclusions

The comparison of sunitinib distributions in *in vivo* animal and *in vitro* experimental models revealed that a single dose treatment was sufficient to localize the drug in tumors as measured by MALDI-MSI. While technical reproducibility was good more variance was found in comparison of tumors identically treated with sunitinib. Increasing amount of drug could be detected through continued treatment. Based on our data presented here we can assume that biological factors in the tumor growth are influencing the levels of sunitinib being detected during the course of treatment.

Applying the experimental model on tumor sections from untreated animals could accurately reproduce the levels of drug obtained in the *in vivo* treated tumors. This suggests that this simple experimental approach may be successfully applied to investigate drug distributions in tissue sections. The possibility of being able to test multiple drugs on the same sample would open up the option of using this new experimental model for testing how drugs penetrate and bind to the tumor most effectively in a tumor biopsy, which in turn may open up the prospects of a more personalized therapy.

Conflict of interest statement

The authors declare no potential conflicts of interest.

References

1. Siegel R, Desantis C, Jemal A (2014) Colorectal cancer statistics, 2014. CA: a cancer journal for clinicians 64 (2):104-117. doi:10.3322/caac.21220

2. Malvezzi M, Bertuccio P, Levi F, La Vecchia C, Negri E (2014) European cancer mortality predictions for the year 2014. Annals of oncology : official journal of the European Society for Medical Oncology / ESMO. doi:10.1093/annonc/mdu138

3. Durko L, Malecka-Panas E (2014) Lifestyle Modifications and Colorectal Cancer. Current Colorectal Cancer Reports 1 (10):45-54

4. Douillard JY, Sobrero A, Carnaghi C, Comella P, Diaz-Rubio E, Santoro A, Van Cutsem E (2003) Metastatic colorectal cancer: integrating irinotecan into combination and sequential chemotherapy. Annals of oncology : official journal of the European Society for Medical Oncology / ESMO 14 Suppl 2:ii7-12

5. Goldberg RM, Sargent DJ, Morton RF, Fuchs CS, Ramanathan RK, Williamson SK, Findlay BP, Pitot HC, Alberts S (2006) Randomized controlled trial of reduced-dose bolus fluorouracil plus leucovorin and irinotecan or infused fluorouracil plus leucovorin and oxaliplatin in patients with previously untreated metastatic colorectal cancer: a North American Intergroup Trial. Journal of clinical oncology : official journal of the American Society of Clinical Oncology 24 (21):3347-3353. doi:10.1200/jco.2006.06.1317

6. Tournigand C, Andre T, Achille E, Lledo G, Flesh M, Mery-Mignard D, Quinaux E, Couteau C, Buyse M, Ganem G, Landi B, Colin P, Louvet C, de Gramont A (2004) FOLFIRI followed by FOLFOX6 or the reverse sequence in advanced colorectal cancer: a randomized GERCOR study. Journal of clinical oncology : official journal of the American Society of Clinical Oncology 22 (2):229-237. doi:10.1200/jco.2004.05.113

7. Hurwitz H, Fehrenbacher L, Novotny W, Cartwright T, Hainsworth J, Heim W, Berlin J, Baron A, Griffing S, Holmgren E, Ferrara N, Fyfe G, Rogers B, Ross R, Kabbinavar F (2004) Bevacizumab plus irinotecan, fluorouracil, and leucovorin for metastatic colorectal cancer. The New England journal of medicine 350 (23):2335-2342. doi:10.1056/NEJMoa032691

8. Yamada Y, Takahari D, Matsumoto H, Baba H, Nakamura M, Yoshida K, Yoshida M, Iwamoto S, Shimada K, Komatsu Y, Sasaki Y, Satoh T, Takahashi K, Mishima H,

Muro K, Watanabe M, Sakata Y, Morita S, Shimada Y, Sugihara K (2013) Leucovorin, fluorouracil, and oxaliplatin plus bevacizumab versus S-1 and oxaliplatin plus bevacizumab in patients with metastatic colorectal cancer (SOFT): an open-label, non-inferiority, randomised phase 3 trial. The lancet oncology 14 (13):1278-1286. doi:10.1016/s1470-2045(13)70490-x

9. Bergers G, Song S, Meyer-Morse N, Bergsland E, Hanahan D (2003) Benefits of targeting both pericytes and endothelial cells in the tumor vasculature with kinase inhibitors. The Journal of clinical investigation 111 (9):1287-1295. doi:10.1172/jci17929

10. Erber R, Thurnher A, Katsen AD, Groth G, Kerger H, Hammes HP, Menger MD, Ullrich A, Vajkoczy P (2004) Combined inhibition of VEGF and PDGF signaling enforces tumor vessel regression by interfering with pericyte-mediated endothelial cell survival mechanisms. FASEB journal : official publication of the Federation of American Societies for Experimental Biology 18 (2):338-340. doi:10.1096/fj.03-0271fje

11. Motzer RJ, Rini BI, Bukowski RM, Curti BD, George DJ, Hudes GR, Redman BG, Margolin Ka, Merchan JR, Wilding G, Ginsberg MS, Bacik J, Kim ST, Baum CM, Michaelson MD (2006) Sunitinib in Patients With MetastaticRenal Cell Carcinoma. JAMA : the journal of the American Medical Association 295 (21):2516-2524

12. George S, Blay JY, Casali PG, Le Cesne A, Stephenson P, Deprimo SE, Harmon CS, Law CN, Morgan JA, Ray-Coquard I, Tassell V, Cohen DP, Demetri GD (2009) Clinical evaluation of continuous daily dosing of sunitinib malate in patients with advanced gastrointestinal stromal tumour after imatinib failure. European journal of cancer (Oxford, England : 1990) 45 (11):1959-1968. doi:10.1016/j.ejca.2009.02.011

13. George S, Blay JY, Casali PG, Le Cesne A, Stephenson P, Deprimo SE, Harmon CS, Law CNJ, Morgan Ja, Ray-Coquard I, Tassell V, Cohen DP, Demetri GD (2009) Clinical evaluation of continuous daily dosing of sunitinib malate in patients with advanced gastrointestinal stromal tumour after imatinib failure. *European journal of cancer* 45 (11):1959-1968

14. Kulke MH, Bendell J, Kvols L, Picus J, Pommier R, Yao J (2011) Evolving diagnostic and treatment strategies for pancreatic neuroendocrine tumors. Journal of hematology & oncology 4:29. doi:10.1186/1756-8722-4-29

15. Norden AD, Drappatz J, Wen PY (2007) Targeted drug therapy for meningiomas. Neurosurgical focus 23 (4):E12. doi:10.3171/foc-07/10/e12

16. Houk BE, Bello CL, Poland B, Rosen LS, Demetri GD, Motzer RJ (2010) Relationship between exposure to sunitinib and efficacyand tolerability endpoints in patients with cancer: resultsof a pharmacokinetic/pharmacodynamic meta-analysis Cancer chemotherapy and pharmacology 66 (2):357-371

17. Novello S, Scagliotti GV, Rosell R, Socinski Ma, Brahmer J, Atkins J, Pallares C, Burgess R, Tye L, Selaru P, Wang E, Chao R, Govindan R (2009) Phase II study of continuous daily sunitinib dosing in patients with previously treated advanced non-small cell lung cancer. *British Journal of Cancer* 101 (9):1543–1548

18. Saltz LB, Rosen LS, Marshall JL, Belt RJ, Hurwitz HI, Eckhardt SG, Bergsland EK, Haller DG, Lockhart AC, Rocha Lima CM, Huang X, DePrimo SE, Chow-Maneval E, Chao RC, Lenz HJ (2007) Phase II trial of sunitinib in patients with metastatic colorectal cancer after failure of standard therapy. Journal of clinical oncology : official journal of the American Society of Clinical Oncology 25 (30):4793-4799. doi:10.1200/jco.2007.12.8637

19. Moss DM, Siccardi M (2014) Optimising nanomedicine pharmacokinetics using PBPK modelling. British journal of pharmacology. doi:10.1111/bph.12604

20. Chaurand P, Schwartz SA, Reyzer ML, Caprioli RM (2005) Imaging Mass Spectrometry: Principles and Potentials. *Toxicologic pathology* 33 (1):92-101

21. Végvári Á, Fehniger TE, Rezeli M, Döme B, Jansson B, Welinder C, Marko-Varga G (2013) Experimental Models to Study Drug Distributions in Tissue Using MALDI Mass Spectrometry Imaging. J Proteome Res 12 (12):5626-5633

22. Troendle FJ, Reddick CD, Yost RA (1999) Detection of pharmaceutical compounds in tissue by matrix-assisted laser desorption/ionization and laser desorption/chemical ionization tandem mass spectrometry with a quadrupole ion trap. J Am Soc Mass Spectrom 10 (12):1315-1321

23. Reyzer ML, Hsieh YS, Ng K, Korfmacher WA, Caprioli RM (2003) Direct analysis of drug candidates in tissue by matrix-assisted laser desorption/ionization mass spectrometry. Journal of Mass Spectrometry 38 (10):1081-1092. doi:10.1002/jms.525

24. Rohner TC, Staab D, Stoeckli M (2005) MALDI mass spectrometric imaging of biological tissue sections. Mech Ageing Dev 126 (1):177-185. doi:10.1016/j.mad.2004.09.032

25. Hsieh Y, Chen J, Korfmacher WA (2007) Mapping pharmaceuticals in tissues using MALDI imaging mass spectrometry. J Pharmacol Toxicol Methods 55 (2):193-200

26. Prideaux B, Stoeckli M (2012) Mass spectrometry imaging for drug distribution studies. Journal of Proteomics 75 (16):4999-5013. doi:10.1016/j.jprot.2012.07.028

27. Källback P, Shariatgorji M, Nilsson A, Andrén PE (2012) Novel mass spectrometry imaging software assisting labeled normalization and quantitation of drugs and neuropeptides directly in tissue sections. Journal of Proteomics 75 (16):4941-4951. doi:http://dx.doi.org/10.1016/j.jprot.2012.07.034

28. Deininger SO, Cornett DS, Paape R, Becker M, Pineau C, Rauser S, Walch A, Wolski E (2011) Normalization in MALDI-TOF imaging datasets of proteins: practical considerations. Analytical and bioanalytical chemistry 401 (1):167-181. doi:10.1007/s00216-011-4929-z

29. Pirman DA, Yost RA (2011) Quantitative tandem mass spectrometric imaging of endogenous acetyl-L-carnitine from piglet brain tissue using an internal standard. Analytical chemistry 83 (22):8575-8581. doi:10.1021/ac201949b

30. Takai N, Tanaka Y, Inazawa K, Saji H (2012) Quantitative analysis of pharmaceutical drug distribution in multiple organs by imaging mass spectrometry. Rapid communications in mass spectrometry : RCM 26 (13):1549-1556. doi:10.1002/rcm.6256

31. Hamm G, Bonnel D, Legouffe R, Pamelard F, Delbos JM, Bouzom F, Stauber J (2012) Quantitative mass spectrometry imaging of propranolol and olanzapine using tissue extinction calculation as normalization factor. J Proteomics 75 (16):4952-4961. doi:10.1016/j.jprot.2012.07.035

32. Groseclose MR, Castellino S (2013) A mimetic tissue model for the quantification of drug distributions by MALDI imaging mass spectrometry. Analytical chemistry 85 (21):10099-10106. doi:10.1021/ac400892z

33. Pirman DA, Reich RF, Kiss A, Heeren RM, Yost RA (2013) Quantitative MALDI tandem mass spectrometric imaging of cocaine from brain tissue with a deuterated internal standard. Analytical chemistry 85 (2):1081-1089. doi:10.1021/ac302960j

34. Takai N, Tanaka Y, Saji H (2014) Quantification of small molecule drugs in biological tissue sections by imaging mass spectrometry using surrogate tissue-based calibration standards. Mass spectrometry (Tokyo, Japan) 3 (1):A0025. doi:10.5702/massspectrometry.A0025

35. Schinkel AH, Wagenaar E, van Deemter L, Mol CA, Borst P (1995) Absence of the mdr1a P-Glycoprotein in mice affects tissue distribution and pharmacokinetics of dexamethasone, digoxin, and cyclosporin A. The Journal of clinical investigation 96 (4):1698-1705. doi:10.1172/jci118214

36. Manea M, Leurs U, Orban E, Baranyai Z, Ohlschlager P, Marquardt A, Schulcz A, Tejeda M, Kapuvari B, Tovari J, Mezo G (2011) Enhanced enzymatic stability and antitumor activity of daunorubicin-GnRH-III bioconjugates modified in position 4. Bioconjugate chemistry 22 (7):1320-1329. doi:10.1021/bc100547p

37. Dome B, Paku S, Somlai B, Timar J (2002) Vascularization of cutaneous melanoma involves vessel co-option and has clinical significance. J Pathol 197 (3):355-362. doi:10.1002/path.1124

38. Fehniger TE, Végvári Á, Rezeli M, Prikk K, Ross P, Dahlbäck M, Edula G, Sepper R, Marko-Varga G (2011) Direct demonstration of tissue uptake of an inhaled drug: proof-of-principle study using matrix-assisted laser desorption ionization mass spectrometry imaging. Anal Chem 83 (21):8329-8336

39. Kuh H, Jang S, Wientjes M (1999) Determinants of Paclitaxel Penetration and Accumulation in Human Solid Tumor. Journal of Pharmacology and experimental therapeutics 290 (2):871-880

40. Annesley TM (2003) Ion suppression in mass spectrometry. Clinical chemistry 49 (7):1041-1044

41. Fujimura Y, Miura D (2014) MALDI Mass Spectrometry Imaging for Visualizing In Situ Metabolism of Endogenous Metabolites and Dietary Phytochemicals. Metabolites 4 (2):319-346

42. Schwandt A, Wood LS, Rini B, Dreicer R (2009) Management of side effects associated with sunitinib therapy for patients with renal cell carcinoma. OncoTargets and therapy 2:51-61
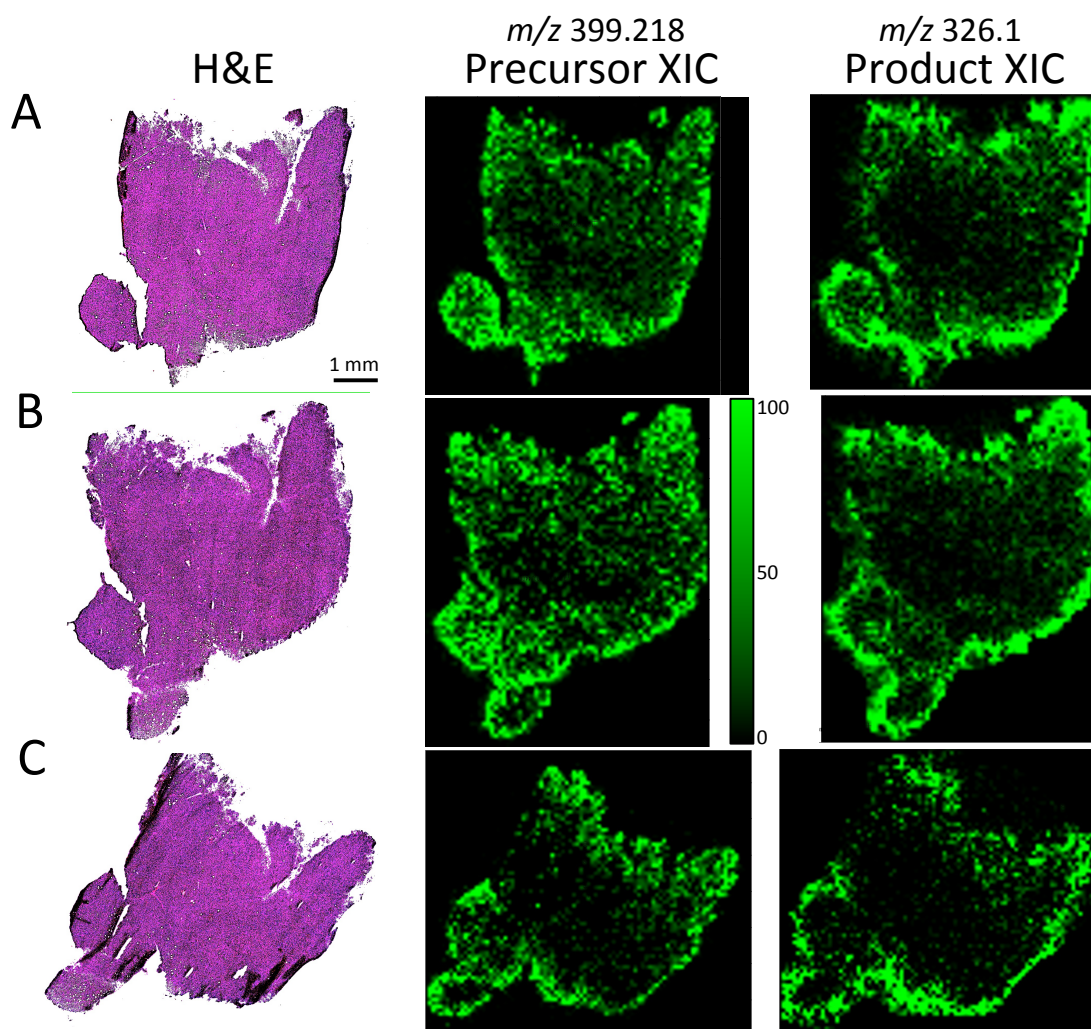
Figure 1. Three technical replicates of a mouse colorectal adenocarcinoma (C-26) treated with a single dose (100 mg/kg) of sunitinib displayed homogeneous distribution of tumor cells (H&E) yet the drug was unevenly localized. The lateral distribution of sunitinib in these adjacent tissue sections showed that more drug molecules were present in the peripheral area than in the center as the precursor mass (*m/z* 399.218) intensities normalized on TIC exposed. The extracted product ion of sunitinib (*m/z* 326.1) presented very similar localization.
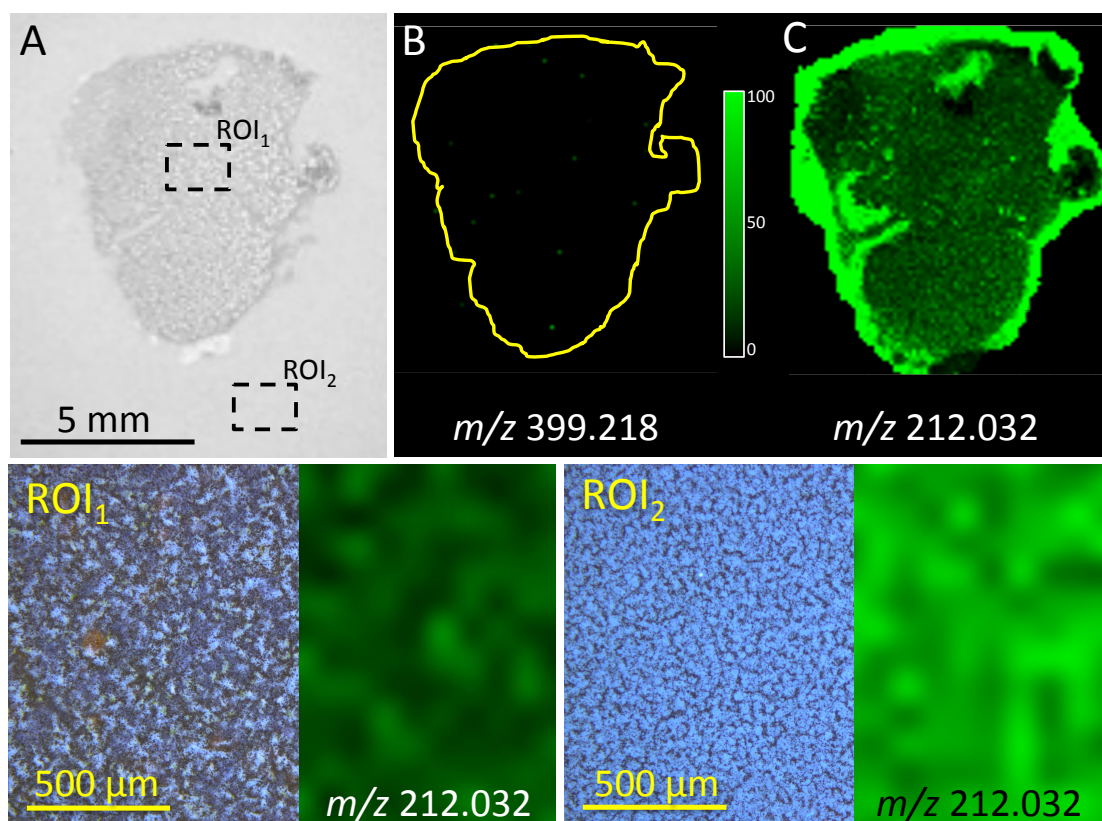
Figure 2. Manual spaying of the matrix over a tissue section of an untreated mouse colorectal adenocarcinoma (C-26) typically provided homogeneous crystallization over the tissue and glass surfaces (A). The untreated tissue displayed no signals of sunitinib in this control experiment (B) but rather homogenous matrix intensities as the Na-adduct of CHCA (m/z 212.032) demonstrated (C). Uniform crystallization was observed on both tissue and glass surface using transmission microscopy (ROI$_1$ and ROI$_2$, respectively). However, the signal intensities of CHCA were significantly lower and less homogenously distributed on the tissue (ROI$_1$) than on the glass surface (ROI$_2$).
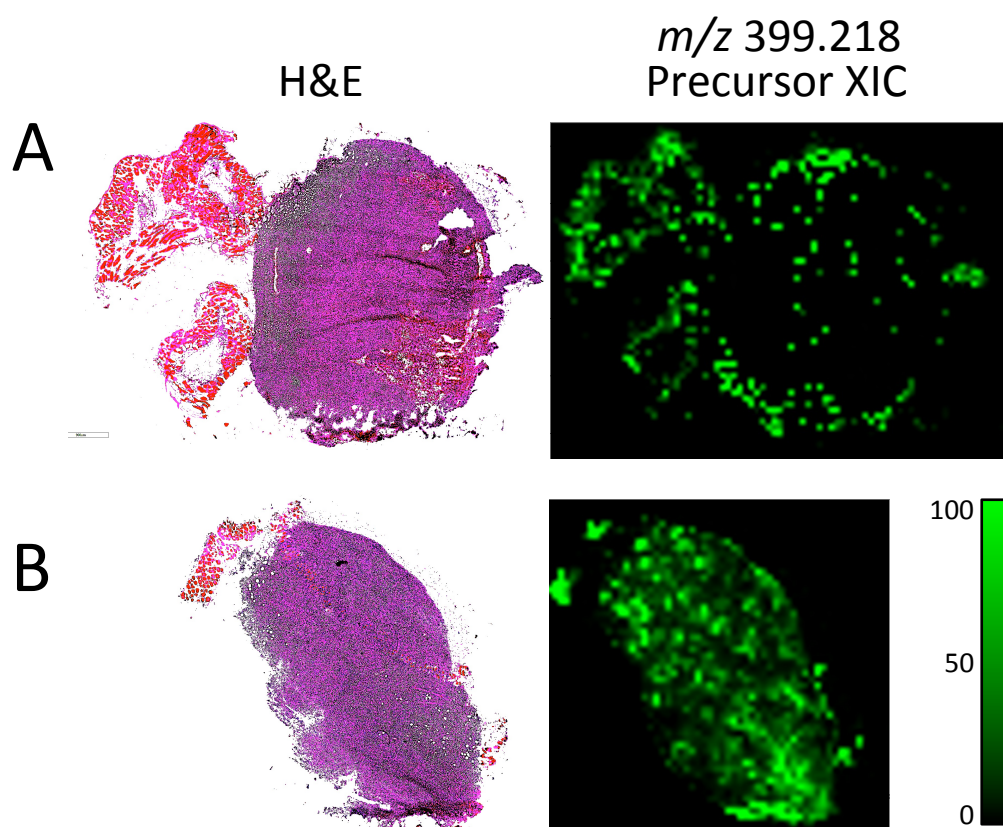
Figure 3. Two additional mouse colorectal adenocarcinomas (C-26) treated with a single dose (100 mg/kg) presented some biological variability as the precursor mass (*m/z* 399.218) intensities normalized on TIC indicated. The tumor cells were homogeneously distributed but their density might be higher in the second tumor (B) that was also supported the higher signal intensities of sunitinib.
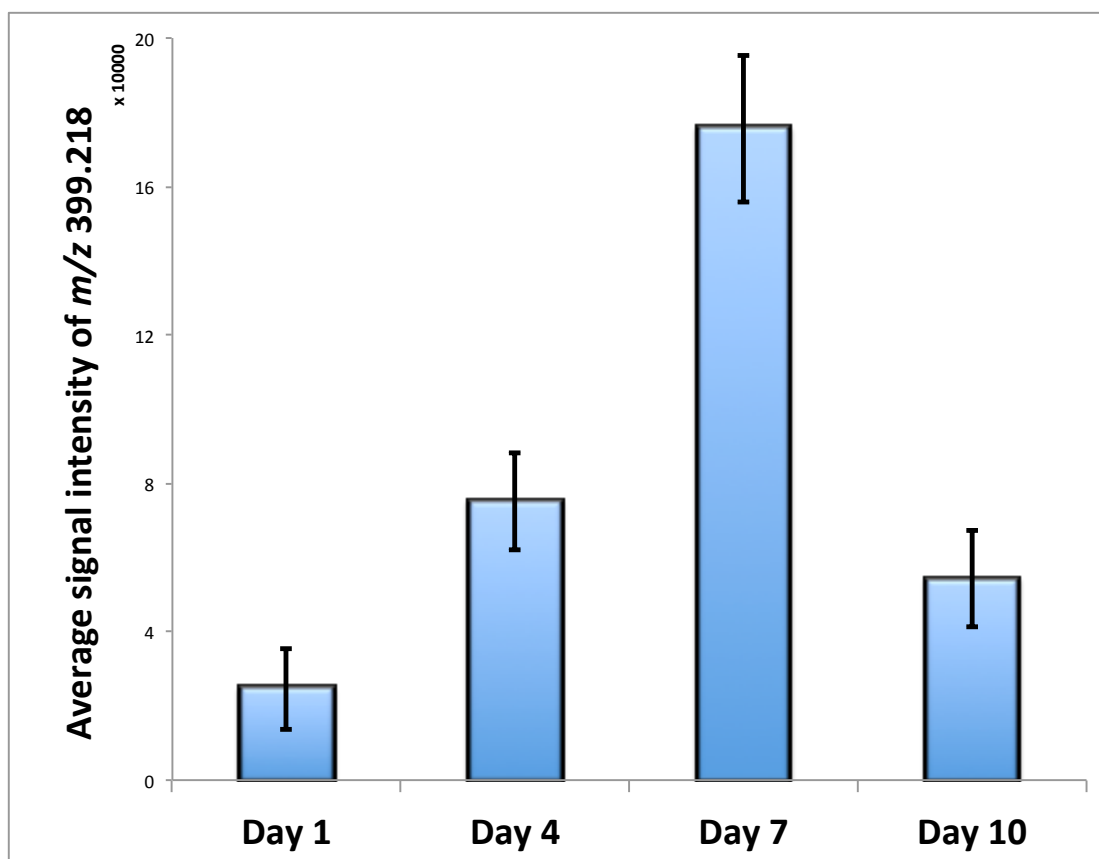
Figure 4. The average signal intensities of sunitinib as calculated from small ROIs within each tissue section (500 analyzed positions) after 1, 4, 7 and 10 days treatment. The estimated levels of sunitinib in treated mouse colorectal adenocarcinomas (C-26) showed fast accumulation of the drug until day seven that was however found to be significantly lower at day 10.
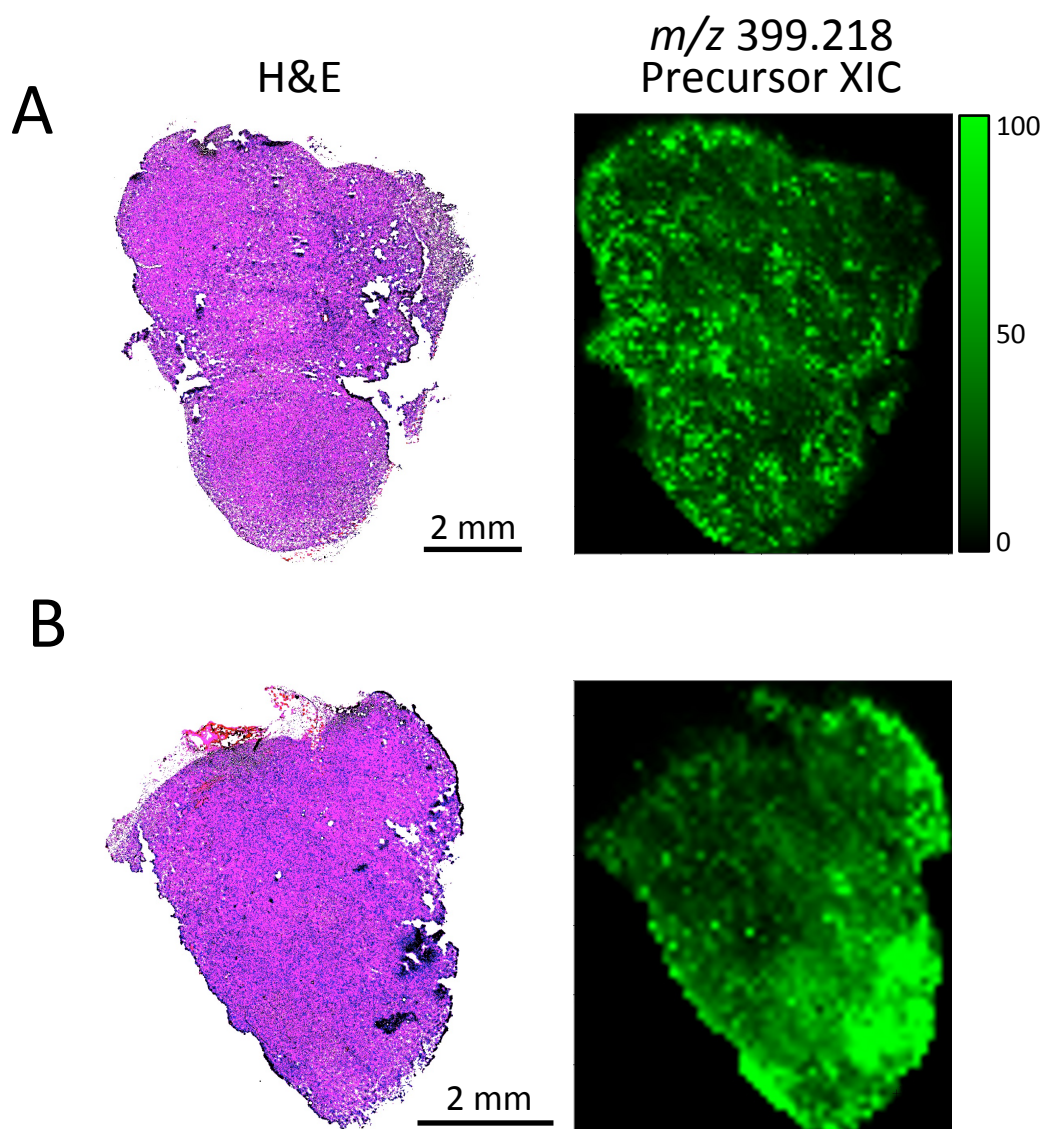
Figure 5. Tissue sections of two untreated mouse colorectal adenocarcinomas (C-26) were exposed to sunitinib using the *in vitro* immerse overlay model presenting detectable levels of the drug. Sunitinib localization appeared to follow the histological structure of the tumor sections.